



Contents lists available at ScienceDirect

Journal of Nuclear Materials

journal homepage: www.elsevier.com/locate/jnucmat

Rapid synthesis of $\text{Pb}_5(\text{VO}_4)_3\text{I}$, for the immobilisation of iodine radioisotopes, by microwave dielectric heating

M.C. Stennett, I.J. Pinnock, N.C. Hyatt*

Immobilisation Science Laboratory, Department of Materials Science and Engineering, The University of Sheffield, Mappin Street, Sheffield S1 3JD, UK

ARTICLE INFO

Article history:

Received 19 February 2011

Accepted 17 April 2011

Available online xxxx

ABSTRACT

Rapid synthesis of $\text{Pb}_5(\text{VO}_4)_3\text{I}$, a potential immobilisation host for iodine radioisotopes, was achieved in an open container by microwave dielectric heating of a mixture of PbO , PbI_2 , and V_2O_5 at a power of 800 W for 180 s (at 2.45 GHz). The resulting ceramic bodies exhibited a zoned microstructure, differentiated by inter-granular porosity and phase assemblage, as a consequence of the inverse temperature gradient characteristic of microwave dielectric heating. Liquid PbI_2 within the interior of microwave processed ceramics assisted formation of $\text{Pb}_5(\text{VO}_4)_3\text{I}$, and reduced inter-granular porosity. In contrast, the exterior of microwave processed ceramics comprised poorly sintered $\text{Pb}_5(\text{VO}_4)_3\text{I}$ with the presence of minor reagent relics. Quantitative microanalysis, electron diffraction and Rietveld analysis, confirmed the synthesis of stoichiometric $\text{Pb}_5(\text{VO}_4)_3\text{I}$ within precision. The crystal structure of $\text{Pb}_5(\text{VO}_4)_3\text{I}$ was found to adopt space group $\text{P}6_3/\text{m}$ with $a = 10.4429(3)$ Å and $c = 7.4865(2)$ Å.

© 2011 Elsevier B.V. All rights reserved.

1. Introduction

A renaissance of interest in nuclear energy has been driven by the desire to reduce dependence on fossil fuels and CO_2 emissions [1]. However, a major expansion of nuclear energy is likely to demand innovative and cost effective improvements to the processing and disposal of spent nuclear fuel and nuclear wastes. Iodine radioisotopes constitute an important fraction of the fission product inventory arising from fission of ^{235}U in thermal reactors. ^{129}I is the most important of these radioisotopes with respect to potential long term dose arising from direct disposal and reprocessing of nuclear fuels and constitutes 0.8% of the total fission product inventory [2]. The high radiotoxicity of ^{129}I arises from the combination of β , γ decay (0.06 MeV β , 0.025 MeV γ), long half life (15.7×10^6 y), high mobility in the environment and accumulation in the human thyroid gland leading to thyroid cancer [2,3]. ^{129}I liberated through reprocessing of nuclear fuels by the Plutonium Uranium Recovery by EXtraction (PUREX) process is typically discharged into the marine environment where dispersal and dilution by natural ^{127}I minimise the potential dose to the general population [2]. However, future regulatory decisions may seek to limit the discharge of ^{129}I , requiring safe and effective long term immobilisation of this radionuclide. The design and processing of suitable containment matrices is complicated, however, by the volatility of elemental iodine, the corrosive nature of iodide salts and facile displacement of the iodide anion by other halide species in ground waters [3].

Audubert et al. proposed lead iodovanadate, $\text{Pb}_5(\text{VO}_4)_3\text{I}$, as a potential immobilisation matrix for the immobilisation of ^{129}I , with a low iodine leach rate of $0.0025 \text{ g m}^{-2} \text{ d}^{-1}$ at pH 6 and 90°C [4]. This compound adopts the apatite structure type, with the large iodide anions immobilised in the one-dimensional tunnels formed by corner sharing VO_4 polyhedra [5], Fig. 1. The solid state synthesis of $\text{Pb}_5(\text{VO}_4)_3\text{I}$ is complicated by the volatilisation of iodine, hitherto necessitating reaction in a closed system between PbI_2 and $\text{Pb}_3(\text{VO}_4)_2$ (the latter precursor prepared by reaction between PbO and NH_4VO_3 or V_2O_5) [4,6,7]. This reaction is generally achieved by hot isostatic or uniaxial pressing of a mixture of $\text{Pb}_3(\text{VO}_4)_2$ and PbI_2 in a sealed metal can for several hours at $500\text{--}700^\circ\text{C}$ and $9\text{--}200$ MPa, alternatively the reaction may be achieved in a sealed quartz vessel [4,6,7]. The synthesis and characterisation of modified iodovanadate phases, $\text{Pb}_5(\text{VO}_4)_{3-x}(\text{PO}_4)_x\text{I}$ and $\text{AgM}_9(\text{VO}_4)_6\text{I}$ ($\text{M} = \text{Pb}, \text{Ba}$), was also reported using the hot isostatic pressing route [8,9]; however, whereas $\text{Pb}_5(\text{VO}_4)_{3-x}(\text{PO}_4)_x\text{I}$ adopts the apatite type structure, $\text{AgM}_9(\text{VO}_4)_6\text{I}$ apparently adopts a different and, as yet undetermined, crystal structure of rhombohedral or monoclinic symmetry. More recently, spark plasma sintering, at $400\text{--}450^\circ\text{C}$ under uniaxial pressure of $30\text{--}70$ MPa, was demonstrated to yield high density ceramic specimens of $\text{Pb}_5(\text{VO}_4)_{2.4}(\text{PO}_4)_{0.6}\text{I}$, either by *in situ* reaction between $\text{Pb}_3(\text{VO}_4)_{1.6}(\text{PO}_4)_{0.4}$ and PbI_2 or consolidation of $\text{Pb}_5(\text{VO}_4)_{2.4}(\text{PO}_4)_{0.6}\text{I}$ prepared *ex situ* in a sealed quartz tube [10,11].

In an effort to develop a simple and rapid synthesis of $\text{Pb}_5(\text{VO}_4)_3\text{I}$ at ambient pressure, without containment, and recognising that V_2O_5 couples extremely efficiently to radiation of domestic microwave frequency (2.45 GHz) [12], we anticipated that direct synthesis of $\text{Pb}_5(\text{VO}_4)_3\text{I}$ could be achieved by microwave

* Corresponding author.

E-mail address: n.c.hyatt@shef.ac.uk (N.C. Hyatt).

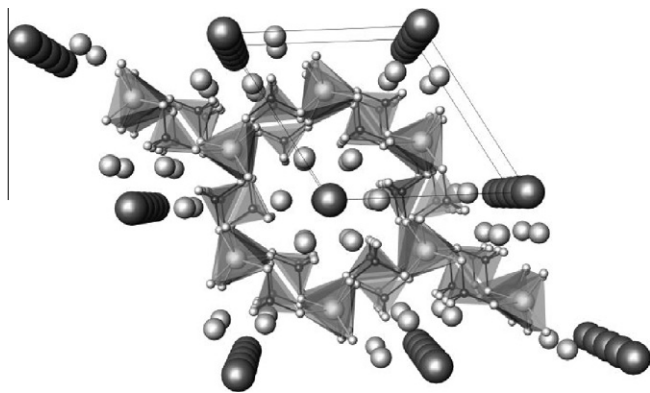


Fig. 1. Schematic representation of the crystal structure of $\text{Pb}_5(\text{VO}_4)_3\text{I}$ determined from X-ray powder diffraction data (Section 3.3), highlighting VO_4 tetrahedra and Pb1 polyhedra; large dark grey spheres represent I, large light grey spheres represent Pb, small black spheres represent V, and small grey spheres represent oxygen; viewed down $[001]$. The unit cell is highlighted.

dielectric heating of a mixture of PbO , V_2O_5 and PbI_2 . Furthermore, the rapid volumetric heating and the inverse temperature profile characteristic of microwave heating [13–16], was anticipated to be advantageous in achieving negligible volatilisation of iodine. The mechanism of microwave dielectric heating involves re-orientation of electric dipoles present in a material, under the influence of an applied electric field at microwave frequency (0.3–300 GHz). If dipole re-orientation does not occur in phase with the microwave field, the resulting phase lag results in a polarisation current within the material. The consequence is resistive heating of the material, as a result of the dielectric loss (i.e. energy dissipation) which is dependent on the phase lag, electric field strength, and polarisation current. In addition, ohmic losses in conductive materials may also contribute to the overall dielectric loss at microwave frequencies. The theory and practice of microwave synthesis and processing of solid state materials has been the subject of several excellent reviews [13–16], to which the reader is referred for comprehensive overview of the subject area. In this contribution we demonstrate the rapid synthesis of $\text{Pb}_5(\text{VO}_4)_3\text{I}$ at ambient pressure in a modified domestic microwave oven.

2. Experimental

The synthesis of $\text{Pb}_5(\text{VO}_4)_3\text{I}$ was attempted by targeting a phase assemblage comprising 90% $\text{Pb}_5(\text{VO}_4)_3\text{I}$ and 10% $\text{Pb}_3(\text{VO}_4)_2$, with the latter phase providing a buffer against potential iodine substoichiometry (as reported by Audubert et al. [4,5]). Appropriate quantities of PbO , PbI_2 , and V_2O_5 were weighed out to give a 20 g batch. The batch was homogenised by ball milling in a 125 ml HDPE pot with 250 g of yttria stabilised zirconia (YSZ) milling media. 20 ml of isopropanol was added as a carrier fluid and the sample was milled for 16 h. After milling, the resulting slurry was passed through a sieve mesh, to separate out the media, and dried at 80 °C for 16 h. The dry powder cake was passed through a 200 μm sieve mesh and stored in a desiccator.

Microwave synthesis experiments utilised a domestic microwave oven, modified to accept a shielded K-type thermocouple, with maximum power output of 800 W and a magnetron frequency of 2.45 GHz, from which the glass turntable and support mechanism were removed. In a typical experiment, 1.00 g of the ball milled reaction mixture, reagent materials, or $\text{Pb}_5(\text{VO}_4)_3\text{I}$, was pressed into a 13 mm diameter pellet, under uniaxial pressure of 50 MPa, and placed in a thin walled alumina crucible (approximately 20 mm diameter and 30 mm tall). The crucible was placed in the centre of an insulating firebrick (of approximate dimensions

$50 \times 50 \times 60$ mm, within a core-drilled cavity (approximately 23 mm diameter, 25 mm deep). The crucible was insulated with refractory wool, inserted to a depth of 15 mm, and covered with an alumina lid. A layer of refractory wool insulation, 25 mm thick, was placed over the fire brick assembly and crucible. The firebrick assembly was positioned at the centre of the microwave oven on small supports fabricated from the same material. Care was taken to ensure the crucible was positioned at the same location (to within ± 5 mm) between experiments. A shielded K-type thermocouple was inserted into a pre-drilled hole within the firebrick to make direct contact with the bottom of the alumina crucible. The reaction temperature was recorded as a function of irradiation time, using a TC08 interface to a PC computer. Samples were irradiated continuously at 800 W (i.e. at full power) for a pre-determined time period up to 500 s.

Accurate temperature measurement during microwave processing is a subject of continuing debate and controversy. It is acknowledged that the use of thermocouple temperature sensors may be problematic since the presence of the thermocouple itself, in some instances, may influence the heating rate and measured temperature. Thermocouple effects were found to be negligible in microwave processing of alumina and zirconia ceramics, with good agreement between the temperature determined by optical pyrometry and thermocouple measurement [17]. Conversely, in a comprehensive study of thermocouple effects on processing of ZnO ceramics, the effects of microwave field distortion, dielectric breakdown and conduction losses were demonstrated to influence thermal and density gradients in the ceramic body during processing under certain conditions [18]. These complications may be circumvented by the use of non-contact temperature measurement devices such as pyrometers and optical fibre sensors. However, such devices are not without disadvantage, including: large minimum spot size, sensitivity to temperature dependence of sample emissivity, surface sensitivity, and cost [18,19]. In the present feasibility study, the large minimum spot size prevented the use of low cost non-contact sensors due to the small scale of the experiments involved. Experiments undertaken in the presence of a thermocouple were repeated using (as far as possible) an identical experimental set up, to assess the potential influence of the thermocouple on the microwave synthesis of $\text{Pb}_5(\text{VO}_4)_3\text{I}$. XRD and SEM/EDX characterisation of samples prepared in the presence and absence of the thermocouple did not reveal any significant variation in the phase assemblage or microstructure of the products. Hence, we conclude that the impact of thermocouple measurement on the microwave reactions reported here is negligible, under the conditions specified.

X-ray powder diffraction data were acquired at room temperature using a Stoe STADI/P diffractometer equipped with a Ge (1 1 1) curved single-crystal monochromator, affording $\text{Cu K}\alpha_1$ radiation and operating in transmission mode. During data collection, specimens, consisting of a thin layer of sample dispersed on Mylar film were rotated in order to alleviate preferred orientation effects. For the purpose of structure refinement studies, the diffraction data were corrected for sample attenuation using the method described by Klug and Alexander [20]. Structure refinement of $\text{Pb}_5(\text{VO}_4)_3\text{I}$ was undertaken using the GSAS suite of programs [21]. All X-ray diffraction data, including that for Rietveld analysis, were acquired on specimens comprising one half of a reacted pellet gently ground to a fine powder in a mortar and pestle, our data are therefore representative of all contributions from the zoned microstructure discussed below.

Cross-sections were prepared for SEM using a low speed diamond saw and mounting in epoxy resin. After curing overnight excess resin was removed using SiC paper (1200 grit) to reveal the sample surface. The surface was then polished to an optical finish (1 μm) using successively finer grades of diamond paste. To avoid

charging in the SEM the surfaces of the samples were sputter coated with carbon. SEM analysis was conducted using a JEOL JSM6400 scanning electron microscope equipped with an Oxford Instruments INCAx-sight energy dispersive X-ray spectrometer for quantitative elemental analysis. Atomic number, absorption and fluorescence (ZAF) correction factors, for each element, were calculated by measuring standards of known composition (V, PbTe and PbI_2). This allowed the measured characteristic X-ray intensities, acquired from spot analyses of the $\text{Pb}_5(\text{VO}_4)_3\text{I}$ samples, to be converted into atom percents. The sample measurement position was fixed and the beam current was calibrated using a cobalt standard mounted flush with the sample in the holder.

Transmission electron microscopy (TEM) was conducted using a Philips EM420 transmission electron microscope operating at 120 kV and a double tilt sample holder. A powder sample was deposited onto a holey carbon film TEM sample grid as a suspension and allowed to dry. Zone axis diffraction patterns (ZADPs) were acquired from several different grains, the composition of the grains were confirmed to correspond to the desired $\text{Pb}_5(\text{VO}_4)_3\text{I}$ phase by EDX analysis using an Oxford Instruments LINK Analytical eXL system.

Analysis of the thermal decomposition of $\text{Pb}_5(\text{VO}_4)_3\text{I}$ was carried out using a Mettler Toledo TGA/DSC1. A powder sample (7.3 mg) was weighed into a 70 μl alumina pan and the sample was heated from room temperature to 900 °C under flowing N_2 at a ramp rate of 10 °C min^{-1} .

3. Results

3.1. Microwave synthesis of $\text{Pb}_5(\text{VO}_4)_3\text{I}$

The relative microwave susceptibility of the reagent materials was determined by measurement of the temperature of a 1.00 g pellet of each substance under microwave irradiation at 800 W for up to 200 s. The results of these experiments are shown in Fig. 2 and demonstrate that V_2O_5 is the effective microwave susceptor in the reaction mixture. Following an initial induction period, the temperature of the V_2O_5 sample was observed to increase smoothly between 30 and 90 s, until the reported melting point of 690 °C was reached at 95 s of irradiation. Above this temperature a rapid increase in heating rate was observed, with the temperature exceeding 1000 °C after a further 15 s of irradiation. Such a “thermal run-away” is typical of many transition metal oxides, for example NiO and Cr_2O_3 [16], with the observed rapid increase of heating rate due to increased dielectric loss at higher

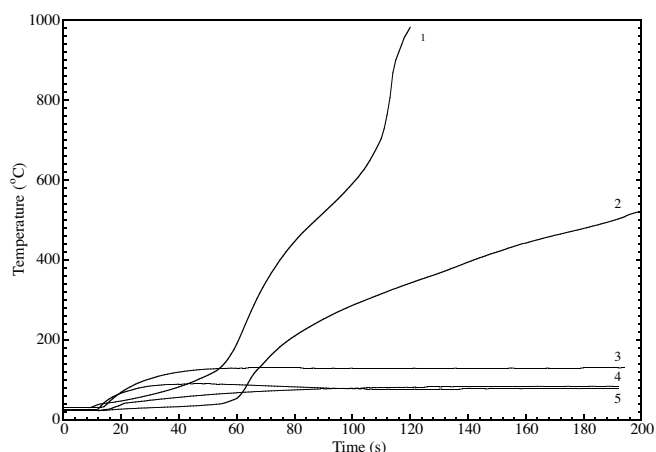


Fig. 2. Temperature as a function of irradiation time at 800 W for 1.00 g specimens of: (1) V_2O_5 , (2) typical reaction mixture to yield 90% $\text{Pb}_5(\text{VO}_4)_3\text{I}$ /10% PbI_2 , (3) PbI_2 , (4) $\text{Pb}_5(\text{VO}_4)_3\text{I}$, and (5) PbO .

temperature. In the case of V_2O_5 , we rationalise the observation of thermal run-away as a likely consequence of ionic diffusion in the molten state which would provide an additional mechanism of dielectric loss at the onset of melting. The microwave susceptibility of PbO , PbI_2 , and $\text{Pb}_5(\text{VO}_4)_3\text{I}$ was found to be poor in comparison to that of V_2O_5 . As shown in Fig. 2, the temperature of PbO , PbI_2 , and $\text{Pb}_5(\text{VO}_4)_3\text{I}$ samples did not exceed 150 °C after 180 s of irradiation at 800 W. We also examined the microwave heating of $\text{Pb}_3(\text{VO}_4)_2$, a potential intermediate in the synthesis of $\text{Pb}_5(\text{VO}_4)_3\text{I}$; however, the temperature of a 1.00 g sample of this material did not exceed 100 °C after 180 s of irradiation at 800 W.

The synthesis of $\text{Pb}_5(\text{VO}_4)_3\text{I}$ was attempted by targeting a phase assemblage comprising 90% $\text{Pb}_5(\text{VO}_4)_3\text{I}$ and 10% $\text{Pb}_3(\text{VO}_4)_2$, with the latter phase providing a buffer against potential iodine substoichiometry (as reported by Audubert et al. [4,5]). Remarkably, powder X-ray diffraction data confirmed the formation of the intended phase assemblage after only 180 s of microwave irradiation at 800 W, as shown in Fig. 3. No significant mass loss was detected at the end of the experiment. At extended reaction times, iodine

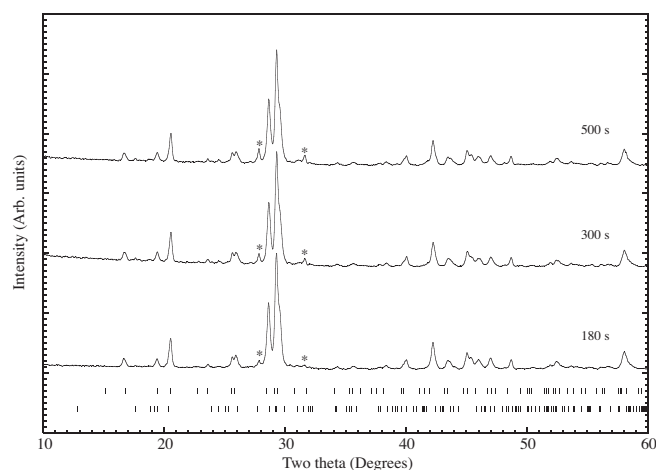


Fig. 3. X-ray powder diffraction patterns of $\text{Pb}_5(\text{VO}_4)_3\text{I}$ samples prepared by microwave irradiation at 800 W for 180, 300 and 500 s. Tick marks show allowed reflections of $\text{Pb}_5(\text{VO}_4)_3\text{I}$ (upper ticks) and $\text{Pb}_3(\text{VO}_4)_2$ (lower ticks); asterisks indicate major observable reflections due to $\text{Pb}_3(\text{VO}_4)_2$.

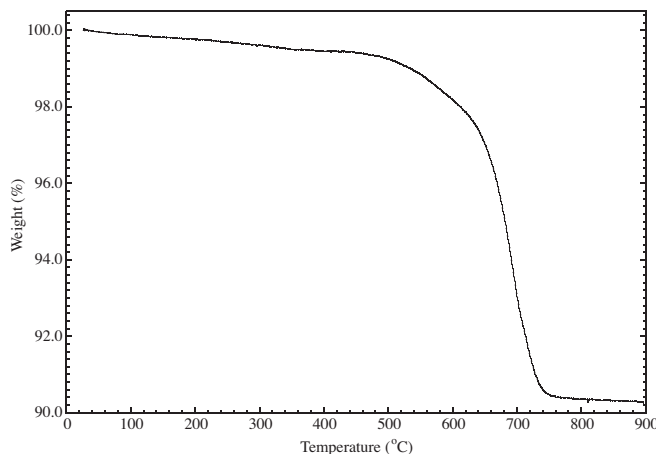


Fig. 4. Thermogravimetric data for a sample comprising 91.8(3)% $\text{Pb}_5(\text{VO}_4)_3\text{I}$ and 8.2(3)% $\text{Pb}_3(\text{VO}_4)_2$ (determined by Rietveld analysis (see Section 3.3)), prepared by microwave irradiation at 800 W for 180 s. Data were acquired under dry N_2 at a heating rate of 10 °C min^{-1} .

vapour was observed during the course of heating which suggested partial decomposition of the $\text{Pb}_5(\text{VO}_4)_3\text{I}$ host phase. This was confirmed by inspection of X-ray powder diffraction patterns which showed an increase in intensity of $\text{Pb}_3(\text{VO}_4)_2$ reflections relative to those of $\text{Pb}_5(\text{VO}_4)_3\text{I}$, as shown in Fig. 3.

The temperature stability of $\text{Pb}_5(\text{VO}_4)_3\text{I}$ was investigated by TGA using a sample prepared by 180 s irradiation at 800 W (comprising 91.8(3)% $\text{Pb}_5(\text{VO}_4)_3\text{I}$ and 8.2(3)% $\text{Pb}_3(\text{VO}_4)_2$, as determined by Rietveld analysis (see Section 3.3)). As shown in Fig. 4, rapid decomposition of $\text{Pb}_5(\text{VO}_4)_3\text{I}$ was observed above 500 °C as a consequence of iodine volatilisation (verified by visual observation). These findings are in agreement with those of Uno et al., who demonstrated $\text{Pb}_5(\text{VO}_4)_3\text{I}$ prepared by hot isostatic pressing to be stable below ~520 °C [6]. The experimentally determined weight loss was 9.7% after heating to 900 °C, which compares reasonably well

with the theoretical weight loss of 7.8% for complete volatilisation of iodine from a phase assemblage comprising 92% of stoichiometric $\text{Pb}_5(\text{VO}_4)_3\text{I}$.

3.2. Ceramic microstructure

Analysis of typical ceramic microstructure was conducted on one quarter cross-section of a pellet processed under microwave irradiation of 800 W for 180 s, (comprising 91.8(3)% $\text{Pb}_5(\text{VO}_4)_3\text{I}$ and 8.2(3)% $\text{Pb}_3(\text{VO}_4)_2$, as determined by Rietveld analysis (see Section 3.3)). Three distinct zones (A–C) were observed in the pellet cross-section, the boundaries of which are highlighted by the dotted lines in the low magnification back scattered electron image of Fig. 5.

Zone A consisted of partially sintered ceramic with large, mainly acicular, voids of the order of 10–20 μm in diameter, as shown in Fig. 6a. The acicular nature of these voids suggests their origin is due to removal of material during mechanical polishing, as a consequence of the friable nature of the specimen, rather than residual porosity. At high magnification in back scattered electron mode, Fig. 6b, a major phase of uniform light grey contrast was observed, with inclusions of a second phase of dark grey contrast a few microns in size. Chemical analysis of the light grey phase by quantitative Energy Dispersive X-ray Spectroscopy (EDX), indicated an average chemical composition consistent with the formation of stoichiometric $\text{Pb}_5(\text{VO}_4)_3\text{I}$. The analysed composition, based on 20 independent point analyses, was: Pb, 23.3(2) at.% (expected 23.8 at.%); V 14.0(1)% (expected 14.3 at.%), and I 4.5(1) at.% (expected: 4.8 at.%). The analysed composition was therefore found to be within three standard deviations of the ideal stoichiometric composition, with no evidence for Pb or I non-stoichiometry. The dark grey inclusions apparent in Fig. 6b were shown by EDX to contain negligible amounts of I and it is considered that these inclusions are $\text{Pb}_3(\text{VO}_4)_2$, confirmed to be present by XRD. Typical EDX spectra from the matrix and inclusions are shown in Fig. 6b. A representative high magnification back scattered electron image of Zone B, is shown in Fig. 7, together with elemental X-ray maps. This zone of the microstructure exhibited percolating inter-granu-

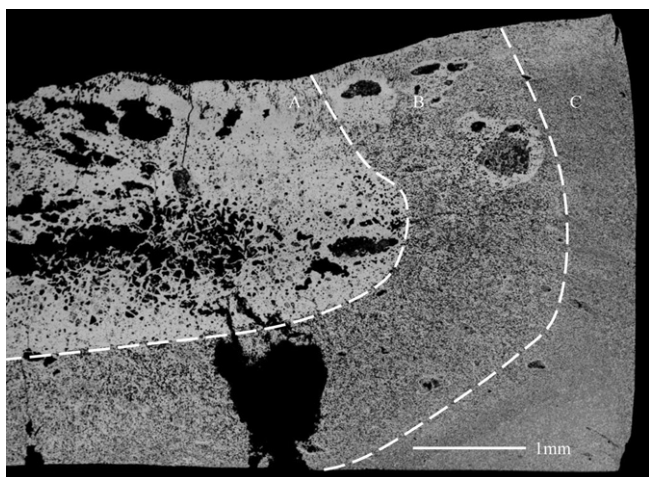


Fig. 5. Low magnification back scattered electron image of cross-section through a sample prepared by microwave irradiation at 800 W for 180 s. Dotted lines indicate boundaries between the different zones of microstructure (A–C), as discussed in the text.

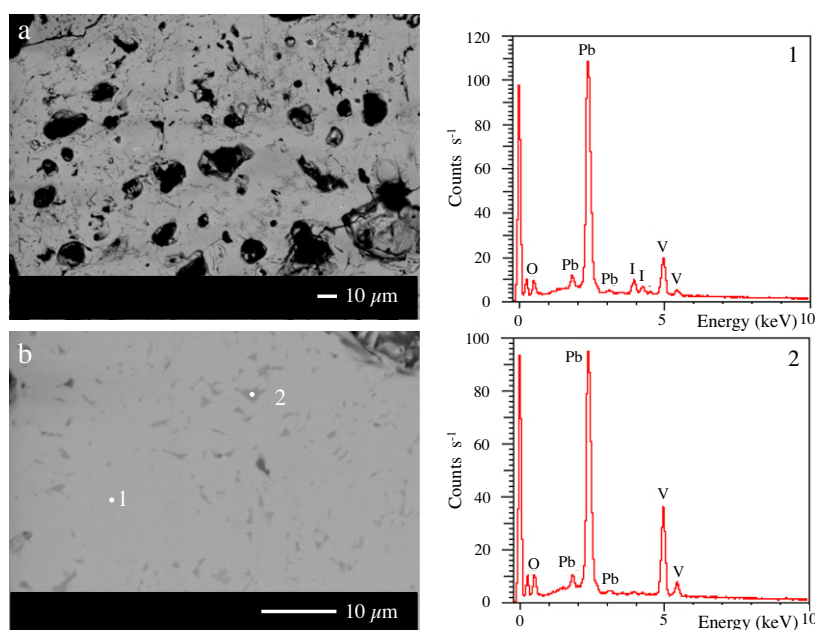


Fig. 6. (a) Low magnification and (b) high magnification back scattered electron images of microstructure in Zone A of a sample prepared by microwave irradiation at 800 W for 180 s (refer to Fig. 5). EDX spectra were acquired at locations 1 and 2, as highlighted, and are representative of the major light grey phase identified as $\text{Pb}_5(\text{VO}_4)_3\text{I}$ and minor dark grey phase identified as $\text{Pb}_3(\text{VO}_4)_2$ (see text for details).

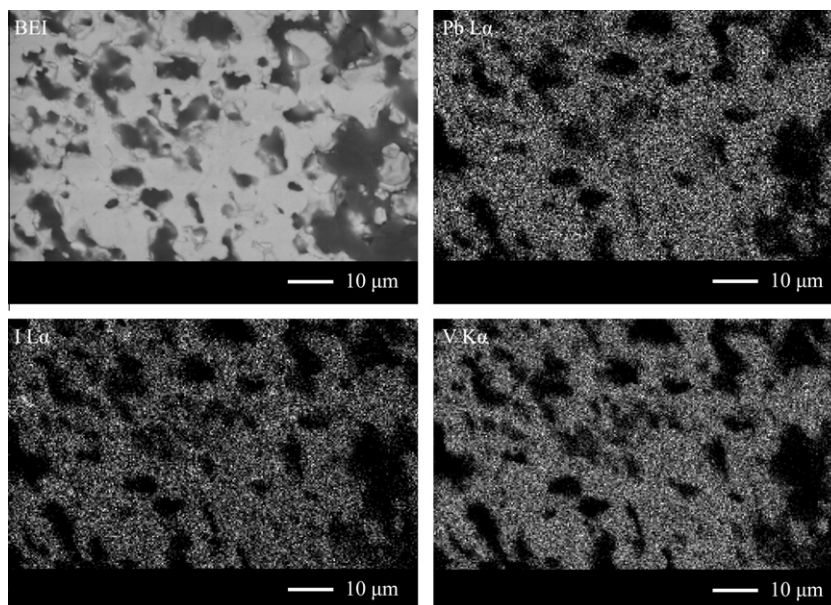


Fig. 7. Back scattered electron image and elemental X-ray maps of microstructure in Zone B of a sample prepared by microwave irradiation at 800 W for 180 s (refer to Fig. 5).

lar porosity characteristic of a poorly sintered ceramic. The uniform grey contrast and elemental X-ray maps demonstrate a homogeneous chemical composition at the micron scale, consistent with the formation of $\text{Pb}_5(\text{VO}_4)_3\text{I}$. Where possible, quantitative EDX analysis revealed this phase to stoichiometric within experimental precision. The microstructure of Zone C, Fig. 8, was found to comprise a poorly sintered assemblage of several phases with considerable inter-granular porosity. The major matrix phase (a) appeared light grey in contrast and was found to comprise Pb, V, and I, in a ratio consistent with $\text{Pb}_5(\text{VO}_4)_3\text{I}$, based on elemental X-ray maps and EDX point analyses. Further analysis of elemental X-ray maps and EDX point analyses suggested the presence of: $\text{Pb}_3(\text{VO}_4)_2$, exhibiting mid-grey contrast (b); V_2O_5 , exhibiting dark grey contrast (c); and two phases exhibiting bright contrast, PbI_2 (d) and PbO (e).

3.3. Structure refinement

Structure refinement studies were undertaken on a sample prepared under microwave irradiation of 800 W for 180 s, comprising 91.8(3)% $\text{Pb}_5(\text{VO}_4)_3\text{I}$ and 8.2(3)% $\text{Pb}_3(\text{VO}_4)_2$, as determined by Rietveld analysis (see below). Quantitative EDX investigation confirmed the formation of stoichiometric $\text{Pb}_5(\text{VO}_4)_3\text{I}$ in this sample, within experimental precision, as discussed above. Typical zone axis electron diffraction patterns collected from $\text{Pb}_5(\text{VO}_4)_3\text{I}$ grains (confirmed by *in situ* EDX characterisation) are shown in Fig. 9. All zone axis diffraction patterns could be successfully indexed based on the $\text{P6}_3/\text{m}$ space group adopted by $\text{Pb}_5(\text{VO}_4)_3\text{X}$ ($\text{X} = \text{F}, \text{Cl}, \text{Br}$) compounds [22–24]. No evidence for additional reflections or diffuse scattering was observed, confirming the absence of additional structural modulation or disorder. Therefore, structure

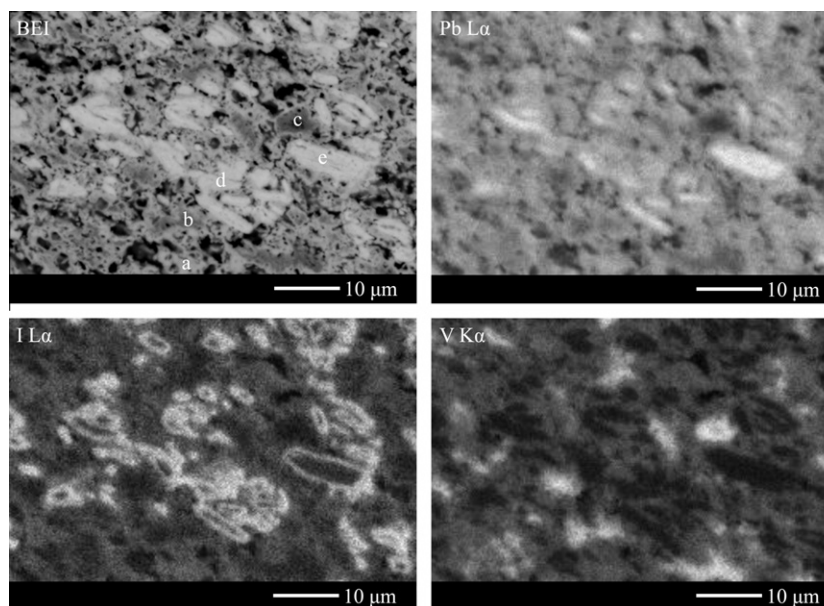


Fig. 8. Back scattered electron image and elemental X-ray maps of microstructure in Zone C of a sample prepared by microwave irradiation at 800 W for 180 s (refer to Fig. 5).

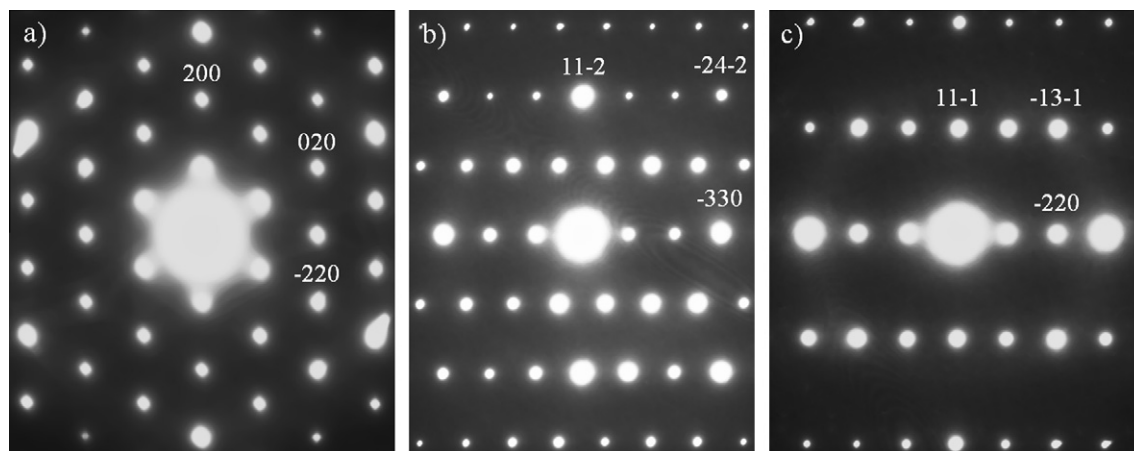


Fig. 9. Indexed zone axis diffraction patterns acquired from $\text{Pb}_5(\text{VO}_4)_3\text{I}$, indexed in space group $\text{P6}_3/\text{m}$: (a) $[0\ 0\ 1]$ zone axis, (b) $[1\ 1\ 1]$ zone axis, (c) $[1\ 1\ 2]$ zone axis.

refinement of $\text{Pb}_5(\text{VO}_4)_3\text{I}$, based on X-ray diffraction data, assumed space group $\text{P6}_3/\text{m}$ and full occupancy of all cation and anion sites in accordance with the experimentally determined composition, which did not reveal significant deviation from ideal stoichiometry within error. $\text{Pb}_3(\text{VO}_4)_2$ ($\text{P2}_1/\text{c}$) was included in the Rietveld analysis as a second phase, the refined phase fraction was 8.2(3)%, in good agreement with the targeted phase assemblage. The refined unit cell parameters of $\text{Pb}_3(\text{VO}_4)_2$ ($a = 7.502(2)\text{ \AA}$, $b = 6.093(2)\text{ \AA}$, $c = 9.539(2)\text{ \AA}$, $\beta = 115.3(2)^\circ$) were in reasonable agreement with those reported previously [25]. Refinement of the structure of $\text{Pb}_5(\text{VO}_4)_3\text{I}$ in $\text{P6}_3/\text{m}$ converged to yield a good fit to the diffraction data, as shown in Fig. 10, with goodness of fit parameters $R_{\text{wp}} = 8.11\%$, $R_p = 5.54\%$, and $\chi^2 = 2.90$ (for a definition of agreement indices see [21,26]). The refined structural parameters are given in Table 1 and key bond lengths are summarised in Table 2. A schematic representation of the crystal structure of $\text{Pb}_5(\text{VO}_4)_3\text{I}$ is shown in Fig. 1.

4. Discussion

4.1. Synthesis

X-ray powder diffraction confirmed the successful synthesis of $\text{Pb}_5(\text{VO}_4)_3\text{I}$ after only 180 s irradiation at 800 W at ambient pressure,

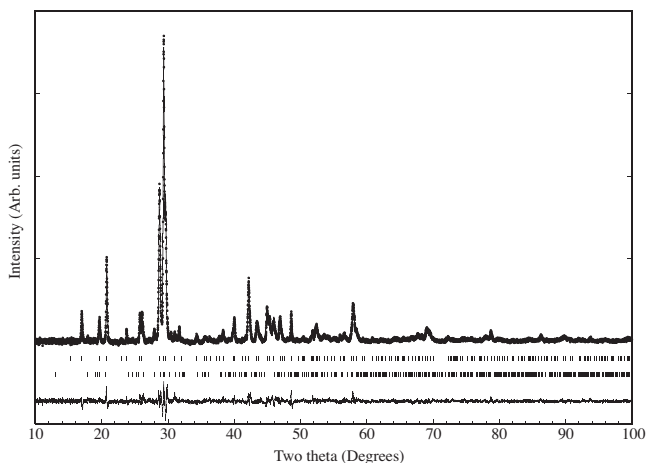


Fig. 10. Showing fit (solid line) to X-ray powder diffraction data (points) for $\text{Pb}_5(\text{VO}_4)_3\text{I}$ at 25 °C in space group $\text{P6}_3/\text{m}$; tick marks show allowed reflections of $\text{Pb}_5(\text{VO}_4)_3\text{I}$ (upper ticks) and $\text{Pb}_3(\text{VO}_4)_2$ (lower ticks); the difference profile (lower solid line) demonstrates a satisfactory fit to the data.

Table 1

Refined structural parameters of $\text{Pb}_5(\text{VO}_4)_3\text{I}$, determined from Rietveld analysis of X-ray powder diffraction data.

Space group		$\text{P6}_3/\text{m}$			
Unit cell parameters		$a = 10.4429(3)\text{ \AA}$		$c = 7.4865(2)\text{ \AA}$	
Atom	Site	x	y	z	$U_{\text{iso}} (x 100\text{ \AA}^2)$
Pb1	4f	1/3	2/3	0.0061(3)	1.04(9)
Pb2	6h	0.2594(1)	0.0101(2)	1/4	1.91(9)
V	6h	0.4121(3)	0.3790(3)	1/4	1.2(2)
O1	6h	1/3	0.491(1)	1/4	1.3(2)
O2	6h	0.606(1)	0.470(1)	1/4	1.1(2)
O3	12i	0.3632(6)	0.271(6)	0.061(6)	1.4(2)
I	2b	0	0	0	1.9(2)

Table 2

Key bond lengths of $\text{Pb}_5(\text{VO}_4)_3\text{I}$ determined from Rietveld analysis of X-ray powder diffraction data.

Bond	Length (Å)
Pb1–O1	2.587(8)
Pb1–O1	2.587(8)
Pb1–O1	2.586(8)
Pb1–O2	2.649(8)
Pb1–O2	2.649(8)
Pb1–O2	2.649(8)
Pb1–O3	2.944(5)
Pb1–O3	2.943(5)
Pb1–O3	2.944(5)
Pb2–O1	3.190(10)
Pb2–O2	2.449(9)
Pb2–O3	2.766(5)
Pb2–O3	2.588(5)
Pb2–O3	2.588(5)
Pb2–O3	2.766(5)
Pb2–I	3.251(5)
Pb2–I	3.251(5)
V–O1	1.73(1)
V–O2	1.75(1)
V–O3	1.72(2)

as demonstrated by Fig. 3. The heating profile of a typical reaction mixture is shown in Fig. 2, following an induction period of approximately 30 s the temperature was observed to increase smoothly reaching $\sim 440\text{ }^\circ\text{C}$ at 180 s; above $520\text{ }^\circ\text{C}$ a small increase in heating rate was observed. TGA analysis demonstrated significant decomposition of $\text{Pb}_5(\text{VO}_4)_3\text{I}$ to occur above $500\text{ }^\circ\text{C}$, increased ionic diffusion as a consequence of iodine volatilisation and phase decomposition would be expected to give rise to enhanced dielectric loss and hence the observed increase in heating rate above $520\text{ }^\circ\text{C}$.

Partial decomposition of $\text{Pb}_5(\text{VO}_4)_3\text{I}$ occurred in samples prepared by irradiation for 300 s and 500 s at 800 W, confirmed by observation of iodine volatilisation and increased phase fraction of $\text{Pb}_3(\text{VO}_4)_2$ inferred from qualitative inspection of reflection intensity ratios in X-ray powder diffraction data (Fig. 3). This conclusion was verified by quantitative phase analysis of X-ray diffraction by whole pattern fitting using crystallographic models for $\text{Pb}_3(\text{VO}_4)_2$ and $\text{Pb}_5(\text{VO}_4)_3\text{I}$ (using the GSAS suite of programs). It was thus determined that the weight fraction of $\text{Pb}_3(\text{VO}_4)_2$ increased from 8.2(3)% after irradiation for 180 s to 15.2(3)% after irradiation for 500 s. The sample temperatures after irradiation at 800 W for 300 s and 500 s were estimated to be 620 °C and 650 °C, respectively. The observed decomposition of $\text{Pb}_5(\text{VO}_4)_3\text{I}$ was therefore consistent with TGA data in which the onset of iodine volatilisation was observed above 520 °C, with the maximum rate of decomposition observed at 690 °C as shown in Fig. 4.

4.2. Microstructure

The zoned microstructure of $\text{Pb}_5(\text{VO}_4)_3\text{I}$ and $\text{Pb}_3(\text{VO}_4)_2$ composite processed for 180 s at 800 W exhibited a partially sintered core, surrounded by zones of residual inter-granular porosity and incomplete reaction. This microstructure is considered a consequence of the inverted temperature profile characteristic of microwave dielectric heating. Following Rao et al. [16], the microwave penetration depth, D , i.e. the distance over which the incident power is reduced to half its initial value, is given by:

$$D = \frac{3\lambda_0}{8.686\pi \tan \delta (\epsilon'')^{1/2}} \quad (1)$$

where $\tan \delta$ and ϵ'' represent the dielectric loss and imaginary permittivity at microwave frequency λ_0 . As shown in Fig. 2, the principle suscepter in the reactions of interest is V_2O_5 , for which $\epsilon'' = 5.43$ and $\tan \delta = 0.68$ at 2.45 GHz and room temperature, as determined by Uematsu et al. [27]. The penetration depth for V_2O_5 at 2.45 GHz is thus estimated to be ~ 10 cm, an order of magnitude greater than the dimension of the sample, leading to volumetric heating. At steady state, however, there is a balance between absorption of microwave radiation by the interior of the sample and radiative loss from the surface. The inverted temperature profile is thus a consequence of rate of heat generation in the pellet core exceeding heat transfer to the pellet periphery.

The combination of volumetric heating and inverted temperature profile is considered critical for the synthesis of $\text{Pb}_5(\text{VO}_4)_3\text{I}$ without the use of a sealed container or over-pressure. Conventional radiant heat transfer relies on absorption of infra-red frequencies in the outer few μm of the sample, resulting in a normal temperature gradient where the surface temperature exceeds that of the interior. Consequently, ceramic $\text{Pb}_5(\text{VO}_4)_3\text{I}$ cannot be prepared by conventional solid state synthesis using radiant heat transfer, without the use of a sealed reaction vessel, because the rate of volatilisation of iodine from the surface exceeds the rate of formation of $\text{Pb}_5(\text{VO}_4)_3\text{I}$ within the sample interior. In the case of microwave irradiation, volumetric heating of the specimen occurs, in a short time scale, leading to quantitative retention of the iodine inventory. A further key point is that the microwave susceptibility of $\text{Pb}_5(\text{VO}_4)_3\text{I}$ at 2.45 GHz is rather poor, even at high temperature. This was demonstrated by failure to re-heat a specimen of $\text{Pb}_5(\text{VO}_4)_3\text{I}$ by microwave irradiation after cooling *in situ* to ~ 300 °C in the absence of the microwave field. Therefore, as V_2O_5 is consumed and $\text{Pb}_5(\text{VO}_4)_3\text{I}$ is formed, the effective microwave susceptibility of the phase assemblage is reduced and the sample does not reach sufficiently high temperature to induce complete decomposition of the target phase by volatilisation of iodine. It should be noted that, as a consequence of the inverse tem-

perature profile, microwave synthesis of $\text{Pb}_5(\text{VO}_4)_3\text{I}$ is sensitive to sample size. In the case of large samples (>3 g), reaction temperatures commonly exceeded 650 °C and complete melting of the sample was observed. This effect could be mitigated by use of a tuneable microwave power source and temperature feedback loop in a purpose designed microwave oven.

The lower inter-granular porosity observed in the interior of microwave processed $\text{Pb}_5(\text{VO}_4)_3\text{I}$ samples, Zone A in Fig. 6, suggests that densification is assisted by formation of a liquid phase. The reaction temperature of ~ 440 °C attained at 180 s was measured by a thermocouple located near to the centre of the lower face of the sample and is hence likely to somewhat underestimate the temperature at the interior centre of the sample. From the melting points of PbI_2 (402 °C), V_2O_5 (696 °C) and PbO (886 °C) [28], we infer the presence of molten PbI_2 at the interior centre of the pellet which may assist rapid formation of $\text{Pb}_5(\text{VO}_4)_3\text{I}$ (from component oxides or intermediates) by enhanced ionic diffusion. It should also be noted that the PbI_2 – PbO phase diagram exhibits a PbI_2 rich eutectic with a melting point of 375 °C, which could also assist liquid phase sintering [29]. Since decomposition of $\text{Pb}_5(\text{VO}_4)_3\text{I}$ is rapid above 520 °C, as demonstrated by TGA analysis (Fig. 4), the formation of this phase within Zone A indicates that the maximum temperature must be below 520 °C: the presence of molten V_2O_5 and PbO is therefore considered unlikely. The presence of substantial residual inter-granular porosity in Zones B and C (Figs. 6 and 7), and minor relics of the reagent materials observed in Zone C (Fig. 7) suggest that if molten PbI_2 assists formation of $\text{Pb}_5(\text{VO}_4)_3\text{I}$ in these zones, then volume of liquid phase must be significantly smaller than at the interior centre of the sample, consistent with the inverse temperature gradient. The elemental X-ray maps shown in Fig. 7, revealed grains of residual V_2O_5 and PbI_2 , together with areas of the target phases $\text{Pb}_5(\text{VO}_4)_3\text{I}$ and $\text{Pb}_3(\text{VO}_4)_2$ (confirmed by spot analyses). The depletion of iodine from the interior of grains which we assume to be PbI_2 relics, and enrichment at the rim, suggests that solid state diffusion of iodine species may be important in Zone C. This could be consistent with (partial) formation of $\text{Pb}_5(\text{VO}_4)_3\text{I}$ by a solid state reaction between V_2O_5 , PbI_2 and $\text{Pb}_3(\text{VO}_4)_2$ in this zone.

4.3. Structure refinement

Analysis of electron diffraction data confirmed $\text{Pb}_5(\text{VO}_4)_3\text{I}$ to adopt space group $\text{P}6_3/\text{m}$, isostructural with $\text{Pb}_5(\text{VO}_4)_3\text{X}$ with $\text{X} = \text{F}, \text{Cl}, \text{Br}$ [22–24]. In particular, we did not observe any evidence for additional super-cell reflections indicating the presence of additional structural modulations as observed in the case of the iodo-oxy apatite $\text{Ca}_{15}(\text{PO}_4)_9\text{IO}$, in which I and O ordering in the tunnel sites leads to a tripling of the unit cell c -axis [30]. The refined crystal structure is in broad agreement with that determined for a phased with composition $\text{Pb}_{4.93}(\text{VO}_4)_3\text{I}_{0.85}$, as reported by Audubert et al. [4,5], although several subtle but significant differences were observed, as discussed below. Note, the previously reported non-stoichiometry would be expected to be detectable within the precision of our quantitative microanalysis.

The crystal structure of $\text{Pb}_5(\text{VO}_4)_3\text{I}$, Fig. 1, may be described as being comprised of corner-linked VO_4 tetrahedra which form one-dimensional channels parallel to the c -axis, in which the large iodide anions are accommodated. The VO_4 tetrahedra are essentially regular with a mean V–O bond length of 1.73 Å, similar to that observed in isostructural $\text{Pb}_5(\text{VO}_4)_3\text{X}$ materials [22–24], and O–V–O bond angles close to the ideal tetrahedral angle: O1–V1–O3, 110.8(3)°, O2–V1–O3, 103.8(4)°, O3–V1–O3, 110.6(4)°. The Pb1 cation adopts a tri-capped trigonal prismatic site, shorter Pb1–O1 (2.59 Å) and Pb1–O2 (2.65 Å) bond lengths are formed with the oxygen atoms forming the trigonal faces of the co-ordination polyhedron, with longer Pb1–O3 bond lengths (2.94 Å) formed with the capping O3

atoms. The Pb²⁺ cation adopts a distorted eight-fold co-ordinate site, involving four near co-planar Pb²⁺–O₃ bonds (mean 2.67 Å), a short apical Pb²⁺–O₂ bond (2.45 Å), a longer Pb²⁺–O₁ bond (3.19 Å), and two equivalent Pb²⁺–I bonds (3.25 Å). The bond valence sums of the V, Pb₁ and Pb₂ cations were determined to be 4.9+, 1.9+ and 2.0+, respectively, confirming satisfactory V–O and Pb–O bond lengths are achieved in the refined structure.

A key difference between the current study and that of Audubert et al., is the stoichiometry of the phase under study. In the present study, no significant deviation from ideal cation stoichiometry was detected by calibrated EDX analysis, within experimental precision. Furthermore, allowing the occupancy of the I and Pb sites to refine, subject to the constraint of overall charge neutrality, provided no evidence for significant deviation from ideal stoichiometry. The unit cell volume reported in this study, 707.07(1) Å³, is significantly larger than that reported by Audubert et al., 702.4(6) Å³, consistent with the absence of detectable Pb and I vacancies. In the structure of Pb_{4.93}(VO₄)₃I_{0.85}, vacancies were observed on the Pb₁ and Pb₂ sites, with the Pb₂ cation displaced from (x, y, ¼) to a 50% occupied (x, y, z) position; this shift was accompanied by displacement of the O₃ and I anions from their ideal positions. Displacement of the O₃ anion resulted in highly distorted VO₄ tetrahedra, with O–V–O bond angles in the range 83(2)–125(2)°. Attempts to model atom displacements in the current study were unsuccessful. The presence of Pb and I vacancies in Pb_{4.93}(VO₄)₃I_{0.85} was rationalised by unfavourable steric interactions between the large iodide anion and Pb²⁺ lone pair, which are both accommodated in the one-dimensional tunnels. The results of the present study do not suggest a requirement for non-stoichiometry in the Pb_{5-x}(VO₄)₃I_{1-2x} solid solution (i.e. x > 0), as previously proposed. In the absence of non-stoichiometry, the structure of Pb₅(VO₄)₃I does not exhibit the distortions observed in Pb_{4.93}(VO₄)₃I_{0.85}; in particular, distortion of the VO₄ tetrahedra are not observed. The isotropic thermal parameters of the Pb₂ and I atoms may suggest small local displacements from the refined ideal positions, however, the absence of detectable diffuse scattering, or additional super-cell reflections, in zone axis electron diffraction patterns (Fig. 9), confirms the absence of even short range correlated atom displacements, in agreement with the outcome of structure refinements discussed above.

5. Conclusions

The rapid synthesis of stoichiometric Pb₅(VO₄)₃I was achieved, without the use of a sealed container, by microwave irradiation at 800 W in a modified domestic microwave operating at 2.45 GHz. Structural characterisation and quantitative microanalysis confirmed the synthesis of stoichiometric Pb₅(VO₄)₃I, it may therefore be concluded that there is no primary requirement of Pb and I non-stoichiometry required to stabilise the structure of this compound as previously proposed. The success of the microwave synthesis methodology is attributed to the rapid volumetric heating of samples arising from the high microwave susceptibility of V₂O₅ at 2.45 GHz. Furthermore, the poor microwave susceptibility of the product phase Pb₅(VO₄)₃I enables the reaction to effectively decouple from the microwave field as V₂O₅ is consumed, which limits the maximum reaction temperature attained and prevents complete decomposition of the desired product by iodine volatilisation. The zoned microstructure of ceramics prepared by microwave processing was rationalised in terms of the inverse temperature gradient characteristic of microwave dielectric heating, where, at steady state, there is balance between absorption of microwave radiation by the interior of the sample and radiative heat loss from the surface. Thus, the temperature of the specimen interior exceeds that of the exterior. The synthesis of Pb₅(VO₄)₃I by microwave dielectric heat-

ing is clearly advantageous in terms of reaction time and self limiting temperature control, without the need to use a sealed reaction vessel or over-pressure to mitigate against iodine volatilisation. We anticipate, therefore, that this methodology may hold particular potential for the immobilisation of volatile radionuclides in ceramic and glass materials. The ceramic bodies produced in this feasibility study would not be suitable for geological disposal due to the porosity apparent in the microstructure and presence of some minor relics of unreacted PbI₂. However, these issues could be addressed in the future by use of a purposed designed microwave reaction cavity, to more effectively insulate the exterior of the specimen, combined with a temperature control and microwave feedback system to regulate the reaction temperature.

Acknowledgements

We are grateful to EPSRC for funding to support the research described in this paper, under Grant EP/F055412/1: Decommissioning, Immobilisation And Management Of Nuclear wastes for Disposal (DIAMOND), and the Nuclear First Doctoral Training Centre for the provision of a research internship to IJP. NCH is grateful to the Royal Academy of Engineering and Nuclear Decommissioning Authority for funding.

References

- [1] R.C. Ewing, *Elements 2* (2006) 331.
- [2] P.D. Wilson, *The Nuclear Fuel Cycle from Ore to Waste*, Oxford University Press, 1996.
- [3] P. Taylor, V.J. Lopata, D.D. Wood, H. Yacyszyn, Solubility and stability of inorganic iodides: candidate wasteforms for iodine-129, in: P.L. Cote, T.M. Gilliam (Eds.), *Environmental Aspects of Stabilisation and Solidification of Hazardous and Radioactive Wastes*, ASTM STP 1033, American Society for Testing and Materials, Philadelphia, 1989, pp. 287–301.
- [4] F. Audubert, J. Carpena, J.L. Lacout, F. Tetard, *Solid State Ionics* 95 (1997) 113.
- [5] F. Audubert, J.M. Savariault, J.L. Lacout, *Acta Crystallogr. C55* (1999) 271.
- [6] M. Uno, M. Shinohara, K. Kurosaki, S. Yamanaka, *J. Nucl. Mater.* 294 (2001) 119.
- [7] E.R. Maddrell, P.K. Abratis, *Mater. Res. Soc. Symp. Proc.* 807 (2004) 261.
- [8] C. Guy, F. Audubert, J.E. Lartigue, C. Latrille, T. Advocat, C. Fillet, *C.R. Phys.* 3 (2002) 827–837.
- [9] M. Uno, A. Kosuga, S. Masuo, M. Imamura, S. Yamanaka, *J. Alloys Compd.* 284 (2004) 300–302.
- [10] L. Campayo, S. Le Gallet, Y. Grin, E. Courtois, F. Bernard, F. Bart, *J. Eur. Ceram. Soc.* 29 (2009) 1477–1484.
- [11] S. Le Gallet, L. Campayo, E. Courtois, S. Hoffmann, Y. Grin, F. Bernard, F. Bart, *J. Nucl. Mater.* 400 (2010) 251–256.
- [12] D.R. Baghurst, D.M.P. Mingos, *Chem. Commun.* 12 (1988) 829–830.
- [13] D.E. Clark, W.H. Sutton, *Annu. Rev. Mater. Sci.* 26 (1996) 299–331.
- [14] J.D. Katz, *Annu. Rev. Mater. Sci.* 22 (1992) 153–170.
- [15] *Microwave Processing of Materials*, National Research Council, Publication NMAB-473, National Academy Press, 1994.
- [16] K.J. Rao, B. Vaidyanathan, M. Ganguli, P.A. Ramakrishnan, *Chem. Mater.* 11 (1999) 882–895.
- [17] D.J. Grellinger, M.A. Janney, Temperature measurement in a 2.45 GHz microwave furnace, in: D.E. Clark, W.R. Tinga, J.R. Laia (Eds.), *Microwaves: Theory and Application in Materials Processing II*, American Ceramic Society, Westerville, OH, 1993, pp. 529–538.
- [18] E. Pert, Y. Carmel, A. Birnboim, T. Olorunoyemi, D. Gershon, J. Calame, I.K. Lloyd, O.C. Wilson, *J. Am. Ceram. Soc.* 84 (2001) 1981–1986.
- [19] T. Durka, G.D. Stefanidis, T. Van Gerven, A. Stankiewicz, *Measur. Sci. Technol.* 21 (2010) 045108.
- [20] H.P. Klug, L.E. Alexander, *X-ray Diffraction Procedures: for Polycrystalline and Amorphous Materials*, Wiley, New York, 1974.
- [21] A.C. Larson, R.B. Von-Dreele, Los Alamos National Laboratory Report No. LA-UR-86-748, 1994.
- [22] Y. Dai, J.M. Hughes, *Can. Mineral.* 27 (1989) 189–192.
- [23] W.E. Baker, *Am. Mineral.* 51 (1966) 1712–1718.
- [24] L. Merker, H. Wondratschek, *Z. Anorg. Allg. Chem.* 300 (1959) 41–52.
- [25] H. Kasatani, T. Umeki, H. Terauchi, *Phase Trans.* 38 (1992) 127–220.
- [26] R.A. Young, Introduction to the Rietveld method, in: R.A. Young (Ed.), *The Rietveld Method*, IUCR and OUP, 1996, pp. 1–38.
- [27] K. Uematsua, K. Todab, M. Sato, *J. Alloys Compd.* 389 (2005) 209–214.
- [28] D.R. Lide (Ed.), *Handbook of Chemistry and Physics*, 75th ed., CRC Press, 1994.
- [29] W. Rolfs, E.A. Secco, U.V. Varadaraju, *Mater. Sci. Eng.* 65 (1984) L5–8.
- [30] P.A. Henning, S. Lidin, V. Petricek, *Acta Crystallogr. B55* (1999) 165–169.